frontiers in Materials

ORIGINAL RESEARCH
published: 28 February 2022
doi: 10.3389/fmats.2021.838736

Effect of Extracted Titanium Tailing Slag on the Properties of Alkali-Activated Fly Ash-Ground Blast Furnace Slag Binder

Shuping Wang[1], *Jingjing Li*[1], *Xiaoxin Yun*[1], *Xuewei Lv*[1], *Yujie Zhao*[2] *and Zhigang Zhang*[3]*

[1]College of Materials Science and Engineering, Chongqing University, Chongqing, China, [2]Pangang Group Engineering Technology Co., Ltd, Panzhihua, China, [3]School of Civil Engineering, Chongqing University, Chongqing, China

The extracted titanium tailings slag (TS) is a by-product of titanium extraction from the blast furnace slag. Its chemical composition is similar to that of ground granulated blast furnace slag (GGBS), but the relatively lower reactivity limited its utilization as a supplementary cementitious material. In this study, the reactivity of TS was improved by mechanical grinding, and the optimum property of finely ground TS was selected to replace fly ash (FA) in the alkali-activated FA-GGBS binder. The influence of TS content on the fluidity, setting time, and compressive strength of the ternary binder was investigated. X-Ray diffraction, Fourier-transform infrared spectroscopy, and scanning electron microscopy were used to analyze the effect of TS on the reaction process. Results showed that the optimum reactivity index of TS was 81.18% at 28 days when it was ground for 15 min in a ball mill. The highest compressive strength of the alkali-activated ternary binder was achieved when the replacement of FA by ground TS was 40%, and its 28-day compressive strength was 49.3 MPa, approximately 22% higher than the binder without TS. The addition of the TS would accelerate the reaction process of binder to form more products, including C-(A)-S-H and gismondine.

Keywords: alkali-activated material, extracted titanium tailings slag, reactivity, mechanical strength, reaction process

OPEN ACCESS

Edited by:
Kequan Yu,
Tongji University, China

Reviewed by:
Jun Liu,
Shenzhen University, China
Lili Kan,
University of Shanghai for Science and Technology, China

***Correspondence:**
Zhigang Zhang
zhangzg@cqu.edu.cn

Specialty section:
This article was submitted to Structural Materials, a section of the journal Frontiers in Materials

Received: *18 December 2021*
Accepted: *29 December 2021*
Published: *28 February 2022*

Citation:
Wang S, Li J, Yun X, Lv X, Zhao Y and Zhang Z (2022) Effect of Extracted Titanium Tailing Slag on the Properties of Alkali-Activated Fly Ash-Ground Blast Furnace Slag Binder. Front. Mater. 8:838736. doi: 10.3389/fmats.2021.838736

1 INTRODUCTION

The extracted titanium tailings slag (TS) was produced from titanium extraction blast furnace slag with high TiO_2 content by a process of high-temperature carbonization and low-temperature selective chlorination (Wang et al., 2008). It is mainly produced in the southwestern area of China, and the annual emission is approximately 90,000 tons at present (Sun et al., 2022). The main elements of TS are Ca, Mg, Al, Fe, Si, and Ti, and its chemical compositions are similar to those of ground granulated blast-furnace slag (GGBS). TS has a glassy structure with latent hydraulic property, indicating the potential application prospect in the field of building materials. However, it also contains mineral phases such as perovskite and diopside, causing a lower reactivity than that of GGBS (Zhang 2018; Yao 2019). Therefore, the utilization is limited.

To improve the utilization, some efforts have been made to prepare building materials including tetracalcium aluminoferrite cement (Hong 2014), porous heat insulation materials (Li et al., 2010), and bricks (Zhu et al., 2010). A few researchers focused on the mechanical grinding to improve the reactivity of industrial wastes due to the mechanical–chemical effect of breaking the Si–O and Al–O

bonds (Mucsi et al., 2015; Kumar et al., 2017). When TS was ground for 30 min, the reactivity index can reach 84% at 150 days. It was also reported that the microstructure of cement paste was more compacted by adding the ground TS, and the amount of $Ca(OH)_2$ can be reduced attributed to the pozzolanic effect; thus, the interface between $Ca(OH)_2$ and other hydration products was not so obvious and the durability of concrete was improved (Zhu et al., 2011).

Alkali activation is also considered as an effective method to produce cementitious materials from latent hydraulic industrial byproducts with substantial mechanical properties, and the emission of CO_2 is thought to be lower than Portland cement (Bumanis et al., 2017; Ameri et al., 2019; Moghadam et al., 2019; Beltrame et al., 2020; Biricik et al., 2021). Meanwhile, alkali-activated cementitious material is more durable than Portland cement when attacked by chemical substances. Many investigations have been conducted on the alkali-activated fly ash (FA), alkali-activated GGBS, and the hybrid binders (Moghadam et al., 2019; John et al., Girija 2021). However, the alkali-activated FA usually showed long setting time and a low strength development rate (Temuujin et al., 2010; Pavithra et al., 2016; Soutsos et al., 2016), while the alkali-activated GGBS exhibits fast setting, high early strength but large drying shrinkage (Liu et al., 2016). In this case, the alkali-activated FA-GGBS, which generally has better performance, is in consideration, and some other types of industrial wastes and chemical agents were also applied to optimize the performance (Nath and Sarker 2014; Kuri et al., 2021; Nishanth and Patil 2021). Zhang et al. (2021) found that the flexural and compressive strength of alkali-activated FA mortars was improved by adding TS at 28 days. The values were 6.8 and 63.2 MPa, respectively, when 20% FA was substituted by TS, showing that TS is effective in promoting the mechanical properties of alkali-activated FA.

In the review, seldom investigation has focused on the influence of TS on the properties of alkali-activated FA-GGBS binders. The fluidity, setting time, strength development, and TS action mechanism in the alkali-activated materials is still unclear. This study aims to improve utilization of TS by mechanical grinding and alkali activation through preparing alkali-activated ternary binder. Since TS has a positive effect in alkali-activated cementitious system, FA was replaced by different contents of TS. The effects of TS content on the setting and hardening properties of alkali-activated ternary system were investigated. Furthermore, X-ray diffraction (XRD), Fourier-transform infrared (FTIR) spectroscopy, and scanning electron microscopy (SEM) were carried out to evaluate the microstructure evolution of the binder.

2 MATERIALS AND METHODS

2.1 Raw Materials

In this study, the fly ash was provided by a local power company. Its density was 2.54 g/cm^3, the specific surface area was 405 m^2/kg, and the 28-day reactivity index was 86.8%. GGBS was supplied by a mineral admixture–making company in Hebei (China). The density was 2.88 g/cm^3, the specific surface area was 431 m^2/kg, and 28-day reactivity index was 103%. TS was obtained from a local titanium dioxide–producing plant. Before being used, TS was oven dried at 105°C for 24 h until the free water was removed, followed by grinding at a ball mill for 15, 30, 45, and 60 min, respectively. Coarse particles larger than 0.075 mm were removed by sieving and the residues were adopted in this study. The chemical composition tested by X-ray fluorescence is listed in **Table 1**. The particle size distribution of materials was analyzed and the results are shown in **Figure 1A**. The D_{50} values of FA, GGBS, and TS were 27.75, 14.03, and 58.56 μm, respectively. Their mineral phases were carried out by using X-ray diffraction (XRD) (**Figure 1B**). It can be seen that all these raw materials were mainly composed of glassy structure that the diffused peaks of TS and SG ranged from 23.5 to 34.9° 2θ, and it appeared at 2θ of 23.3–36.9° for FA. In addition, TS contained crystalline structure including wuestite (d-spacings of 0.248, 0.215, and 0.152 nm). Quartz (d-spacings of 0.333 nm) and mullite (d-spacings of 0.537, 0.342, 0.338, and 0.269 nm) were involved in FA, and zoisite was contained in GGBS.

TABLE 1 | Chemical composition of raw materials (wt.%)

	SiO_2	Al_2O_3	CaO	Na_2O	Fe_2O_3	MgO	Cl	TiO_2
FA	42.7	27.1	3.3	2.5	5.8	2.7	—	—
GGBS	35.06	14.42	38.66	0.43	0.34	7.93	—	—
TS	30.75	13.61	29.12	0.42	1.7	8.55	4.98	10.89

The alkali activator used for preparation of the alkali-activated cementitious material was water glass (sodium silicate solution) with moduli (n, SiO_2/Na_2O molar ratio) of 1.2.17.57 g sodium hydroxide (NaOH) tablets that were dissolved directly into 100 g commercial water glass with modulus of 2.57 to adjust the modulus to 1.2. The content of Na_2O, SiO_2, and H_2O of the original water glass was 11.91, 29.64, and 33.19%, respectively. The amount of water, which should be added to the water glass, was determined by the Na_2O equivalent content (mass ratio of Na_2O to solid materials = 12%) and the water to solid mass ratio (w/s = 0.4) of the paste. These materials were mixed homogeneously and kept for more than 24 h to make the alkali solution equivalently.

2.2 Experimental Methods

2.2.1 Preparation of Alkali-Activated Materials

The alkali-activated cementitious material was prepared by mixing the solid materials and alkali solution. In terms of the reference sample, the weight ratio between FA and GGBS was 7:3. The solid materials were mixed homogeneously for approximately 1 min before alkali solution was added in the mixture to prepare a paste. FA was replaced by TS with weight ratios ranging from 10 to 70% to investigate its influence on the setting and hardening properties of the paste. The paste was poured into cubic molds with a size of 40 × 40 × 40 mm and cured at the standard condition with temperature of 20±2°C and relative humidity (RH) ≥95%.

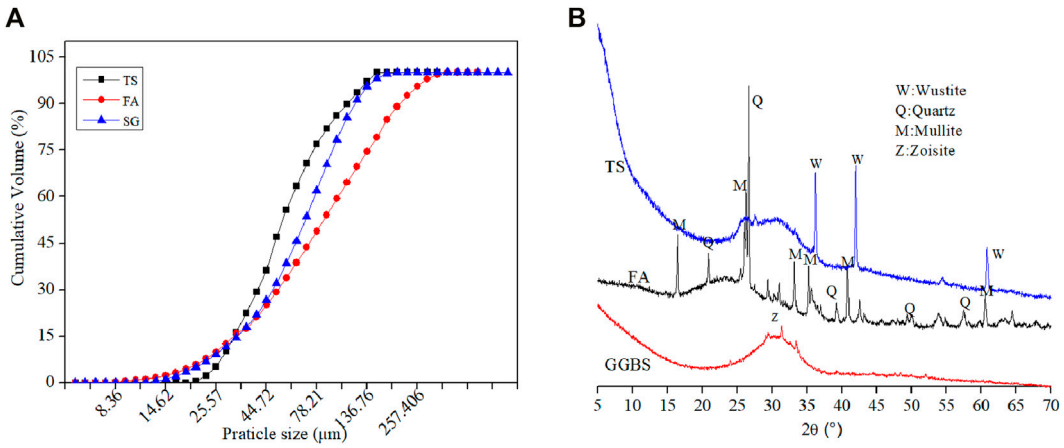

FIGURE 1 | (A) The particle size distribution and **(B)** XRD patterns of the raw materials.

2.2.2 Performance Test

The particle size distribution of FA, GGBS, and TS was analyzed using a Mastersizer 2000 laser diffraction analyzer. The specific surface area was measured by Blaine specific surface area tester according to the Chinese Standard GB/T 8074-2008 (GB/T 8074, 2008). The reactivity of these materials was measured following the Standard GB/T 1596-2017 (GB/T 1596, 2017). It was evaluated by the compressive strength ratios of blended cement mortar (70% Portland cement blended with 30% TS) to the Portland cement mortar at 7 and 28 days of curing, respectively. Setting time of the alkali-activated cementitious material was measured at 20±2°C complying with GB/T 1346-2011 (GB/T 1346, 2011). The initial setting time was determined when the penetration depth of the initial setting needle was 36 ± 1 mm. The fluidity of alkali-activated cementitious material was tested according to GB/T 8077-2000 (GB/T 8077, 2000). The paste was poured into a mini-slump cone, and then the cone was lifted to allow the paste to flow freely for 30 s. The diameters of the spread were measured in two perpendicular directions, and the average value was the fluidity. Compressive strength of the hardened paste being cured at 20 ± 2°C with RH ≥95% for 1, 3, and 28 days was measured by a hydraulic universal testing machine following the Standard GB/T 17671-1999 (GB/T 17671, 1999).

2.2.3 Microstructure Characterization

The sample at different curing ages was collected and immersed in ethanol for 7 days to stop its hydration. Humid samples were then dried at 45°C in a vacuum for 7 days before the microstructure analysis. The dried samples were ground in an agate bowl by hand, and the ground powders smaller than 0.075 mm were retained for XRD and FTIR testing. The mineral phases of the alkali-activated cementitious materials were analyzed by X-ray powder diffraction (XRD; PANalytical X'Pert Powder). The scanning range of 2θ was from 5 to 70°, and the scanning rate was 2°/min with a step of 0.02°. The functional groups of the hydration products of the alkali-activated cementitious material were characterized by FTIR spectroscopy (Nicolet iS50). SEM (Quattro S) was applied to investigate the morphology of the alkali-activated cementitious material. Before measurement, the dried samples were coated in gold with a thickness of approximately 20 nm to improve the electronic conductivity.

3 RESULTS AND DISCUSSIONS

3.1 Influence of Mechanical Grinding on the Performance of TS

3.1.1 Particle Size

The influence of mechanical grinding on the particle size distribution of TS is shown in **Figure 2**. Initially, the fineness of the extracted titanium tailings slag was increased with increasing grinding time, followed by an obvious decrease. The minimum particle size of TS was achieved when the grinding time was 15 min. The particle sizes of D_{10}, D_{25}, D_{50}, D_{75}, and D_{90} were 23.69, 31.91, 48.31, 69.16, and 82.89 μm, respectively.

3.1.2 Reactivity

The reactivity index of the TS in **Figure 3** showed a similar tendency that the value increased first and then decreased with increasing grinding time. When the grinding time was 15 min, the reactivity index was greatly improved and the values of 7- and 28-day reactivity index were 42.60 and 81.18%, respectively. However, when the grinding time increased to 60 min, the values of 7- and 28-day reactivity index decreased to 34.65 and 63.75%. The initial increase in reactivity can be

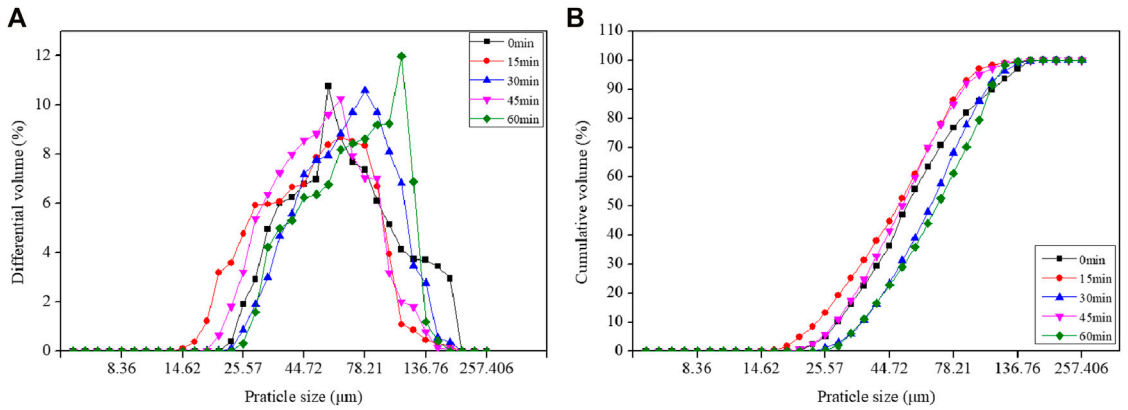

FIGURE 2 | Influence of different grinding times on the **(A)** differential volume and **(B)** cumulative volume of TS.

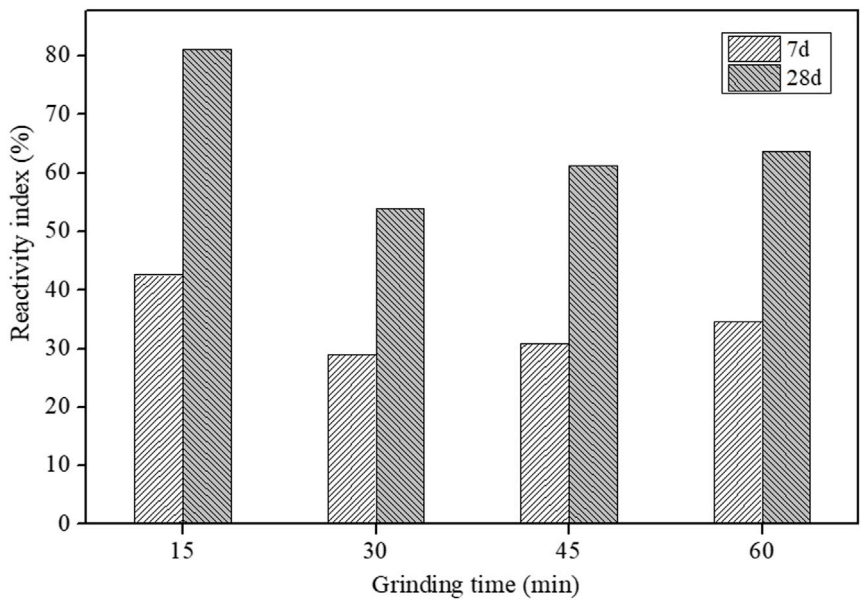

FIGURE 3 | Effect of grinding time on the reactivity of TS.

attributed to the mechanical grinding of refined particles and optimization of the particle gradation in cement paste. In addition, the glassy structure was destroyed and the surface area of TS particles involved in the chemical reaction increased, which is beneficial to silicon and aluminum dissolving and ion penetration in the cementitious system. In addition, the particle lattice was distorted with breakage of the Si–O and Al–O bonds in the network, the structure became disordered, and the number of charged particles increased, and as a consequence, the reactivity increased. The decrease in the reactivity when the grinding time exceeded 15 min was probably due to the aggregation of fine particles into coarser size by further grinding. With respect to the energy consumption during grinding, therefore, the grinding time of 15 min was applied on TS for the preparation of alkali-activated binder in this study.

3.2 The Effect of TS on the Properties of Alkali-Activated FA-GGBS Binder

3.2.1 Fluidity

It can be seen from **Figure 4** that TS played an important role in changing the fluidity of the binder. The initial fluidity (L0 in the figure) of the reference sample (without TS) was 265 mm, and it increased by 5.7% to 280 mm as the content of TS in the alkali-activated materials increased to 40%. An apparent decrease of the

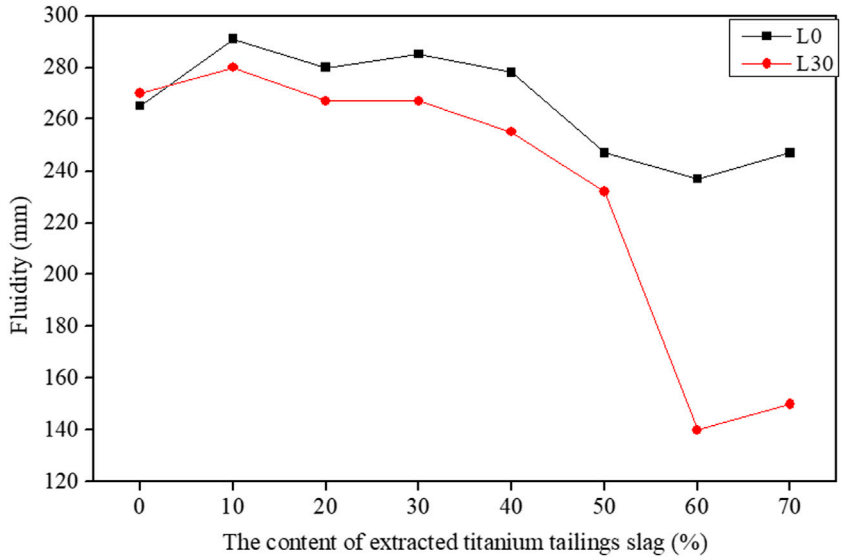

FIGURE 4 | Influence of TS content on the fluidity of the alkali-activated ternary binders.

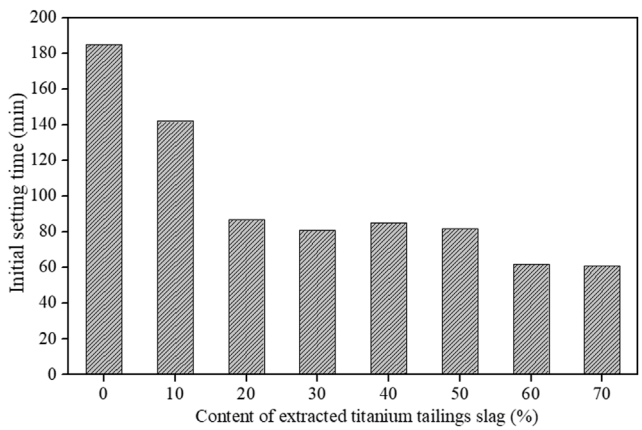

FIGURE 5 | Influence of TS content on the setting time of the alkali-activated ternary binders.

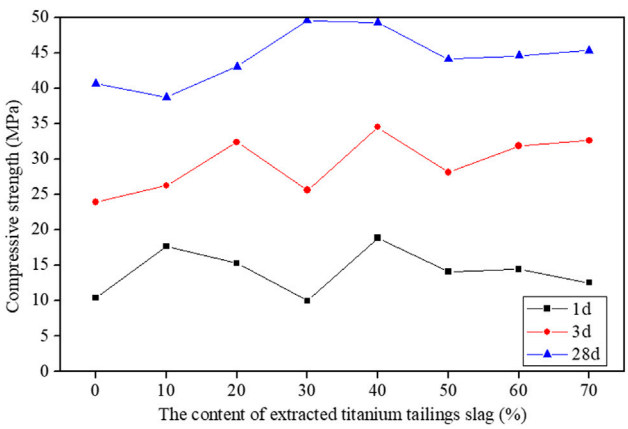

FIGURE 6 | Influence of TS content on the compressive strength of alkali-activated ternary binders.

initial fluidity was observed when the TS content increased from 40 to 70%. In terms of the fluidity at 30 min (L30 in the figure), a slight increase occurred when TS content increased to 10%, followed by a subtle decrease with increasing TS content to 40%. The value of fluidity at 30 min (without TS) was 270 mm, and it decreased by 5.5% to 255 mm at the TS content of 40%. The substantial decrease appeared as the TS content increased from 40 to 70%. The increase in the fluidity at a relatively lower content of TS was likely due to the smaller specific surface area of TS than FA, which reduced the water demand of the mixture. In this case, the amount of free water and the thickness of water film on the particles increased, and thereby the fluidity of the mixture was improved (Xiang et al., 2019). Compared with that of the reference sample, the alkali-activated materials with 60% TS had the lowest values of the initial fluidity and fluidity at 30 min, which was decreased by 11 and 48% to 240 and 140 mm, respectively. A probable reason was that the increased amount of Ca^{2+} in the TS accelerated the reaction process, and the gelation of the binder was accelerated to form calcium silicate hydrate gel (C-S-H) and calcium aluminosilicate hydrate gel (C-A-S-H) (Yip et al., 2005; Rakngan et al., 2018; Song et al., 2019).

3.2.2 Setting Time

Figure 5 shows the influence of TS content on initial setting time of alkali-activated ternary binders. It can be seen that adding TS can shorten initial setting time evidently. Generally, the initial setting times decreased with the increment of TS content. The setting time of alkali-activated ternary binder decreased sharply as the content of TS increased to 40%. The initial setting time was

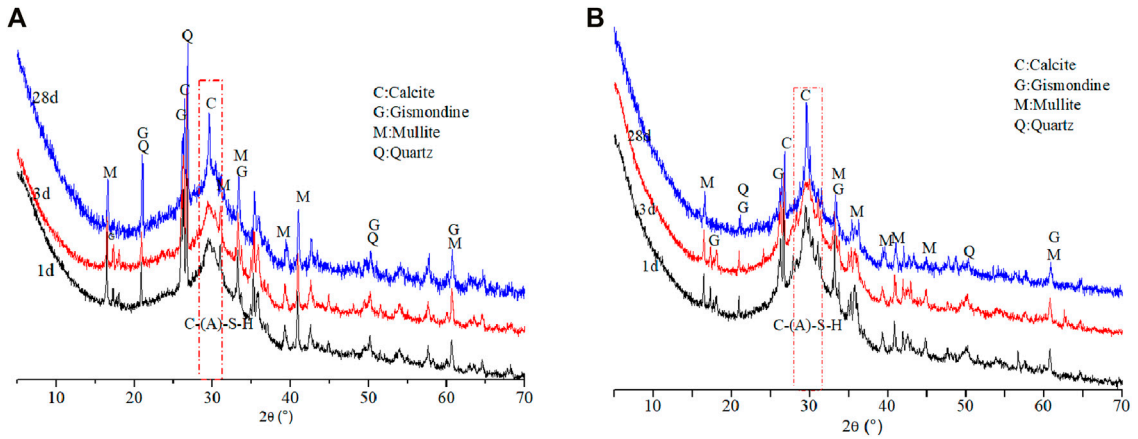

FIGURE 7 | XRD patterns of alkali-activated binders with different compositions at different curing ages: **(A)** 70%FA:30%SG; **(B)** 30%FA:30%GGBS:40%TS.

185 min without TS, and it decreased by 54% to 85 min at the TS-to-FA replacement ratio of 40%. When the TS content in the binder was higher than 40%, a slight diminishment was observed in initial setting time, and the value was 61 min at 70% TS. That is because the setting time is highly related to the amount of reaction products, such as C-A-S-H or C-S-H gels (Chindaprasirt et al., 2011; Cui et al., 2017). Increasing the amount of TS was equivalent to increase the content of calcium oxide in the ternary system, thus accelerating the formation of C-S-H and C-A-S-H gel, and subsequently shortening the setting time (Nath and Sarker 2014; Nath et al., 2015; Nishanth and Patil 2021).

3.2.3 Compressive Strength

The effect of TS on the compressive strength of the alkali-activated ternary binder is shown in **Figure 6**. It can be seen that the replacement of FA by TS generally improved the compressive strength of alkali-activated material, and the compressive strength increased first and then decreased with increasing TS content. The maximum compressive strength of the binder at early ages was achieved as TS content is 40%. Its compressive strength at 1, 3, and 28 days was 18.9, 34.5, and 49.3 MPa, respectively, which was increased by 80.77, 30.72, and 21.18%, respectively, as compared with reference samples without TS addition. This mixture was deemed to have the optimum particle gradation that forms a more compacted structure than the other mixtures, which contributes to the gaining of compressive strength. Apart of the sodium aluminosilicate hydrate gel (N-A-S-H) formed from the reaction between FA and alkali solution, the replacement of FA by TS in the binder system is likely to incorporate more Ca^{2+} ions to produce C-(A)-S-H gel. The combination of C-(A)-S-H and N-A-S-H gels tends to the optimization of pore structure, and resulted in the growth of compressive strength. However, excessive amount of TS was negative to the compressive strength of binder, which is mainly because the reaction between solid materials and alkali solution was accelerated, and subsequent superfluous C-(A)-S-H gel formed in a relatively shorter time. It is likely to initiate cracks in the specimens as a result of the easy loss of gel water, which adversely affected the strength development (Cui et al., 2017).

3.3 Microstructure Analysis

3.3.1 XRD Analysis

The XRD patterns of specimens at different ages are shown in **Figure 7**. It can be seen that the main reaction products were C-(A)-S-H gel with diffused peak ranging from 25 to 35° 2θ and gismondine (d-spacings of 0.427, 0.334, and 0.299 nm) (Chindaprasirt et al., 2012). Mullite (d-spacings of 0.534, 0.287, and 0.269 nm) and quartz (d-spacings of 0.537, 0.342, and 0.338 nm) derived from the raw materials were still present in all the samples at different ages. In addition, calcite (d-spacings of 0.386, 0.303, and 0.283 nm) was also detected, which was probably due to the carbonation of C-(A)-S-H gel. The peak intensity of mullite and quartz decreased with the increase of curing age. Meanwhile, the peak intensity of reaction products (e.g., C-(A)-S-H and gismondine) were stronger and sharper, suggesting the formation of new phase due to the occurrence of reaction between the raw materials and alkali solution. Furthermore, it is found that the peak intensity of mullite and quartz of the samples with addition of TS in **Figure 7B** became weaker than that of reference sample (**Figure 7A**), which is ascribed to the decreased amount of FA, while the peak intensity of C-(A)-S-H in the former sample were stronger and sharper. It indicates that the replacement of FA by TS can promote the formation of C-(A)-S-H gels, and reaction process proceeded with the increase of curing age.

3.3.2 FTIR Spectrum

Figure 8 shows the FTIR spectrum of the alkali-activated binder with different compositions. The bands at the region of 1,600–4,000 cm^{-1} were an indication of hydrogen stretching vibration groups (Si–O–H). The vibration at 3,445 and 1,647 cm^{-1} was attributed to the bending of the hydroxyl band. These bands indicated the presence of bound water molecules from the reaction products. For the reference sample (**Figure 8A**), the

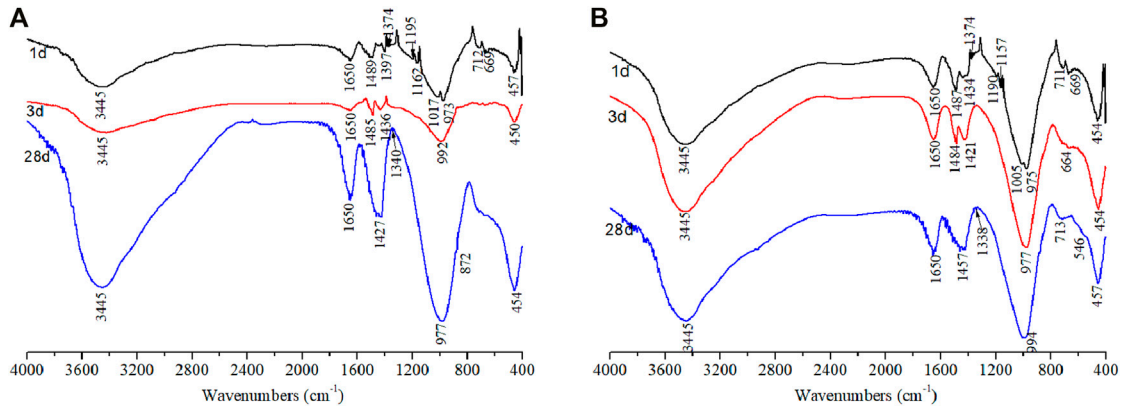

FIGURE 8 | FTIR of alkali-activated binders cured at different ages: **(A)** 70%FA:30%SG; **(B)** 30%FA:30%GGBS:40%TS.

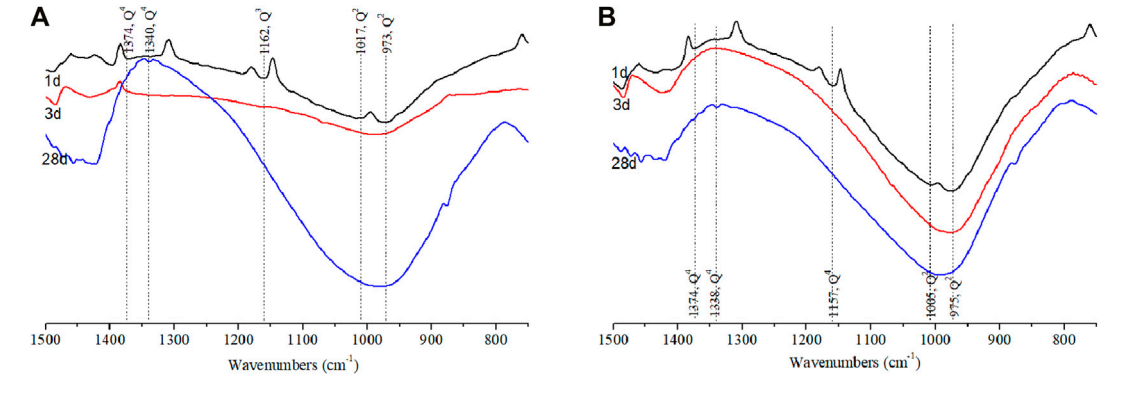

FIGURE 9 | FTIR (450–1,500 cm^{-1}) of alkali-activated binders cured at different ages **(A)** 70%FA:30%SG; **(B)** 30%FA:30%GGBS:40%TS.

increased vibration intensity in the region of 2,000–4,000 cm^{-1} indicated the increased amount of C-(A)-S-H over the curing age. It was low at 1 and 3 days, but increased dramatically at 28 days, indicating a relatively low reaction rate at early ages, and the reaction improved at a later age, whereas a slight increase of intensity in the hydrogen bond vibration was observed with TS addition. The bands at the region of 1,400–1,500 cm^{-1} were the signal of asymmetric stretching vibration of CO_3^{2-}. In addition, the band position at 872 cm^{-1} is due to the bending vibration of the C–O bond of carbonates. The bands positioned at 700–950 cm^{-1} and 400–500 cm^{-1} were the signals of $[AlO_4]^{5-}$ tetrahedron and $[AlO_6]^{9-}$ octahedron, respectively.

The most important bands positioned in the range of 750–1,400 cm^{-1} are related to the stretching vibration of Si–O–T (where T = Si, Al, Ti, and Na etc.) (Liu et al., 2020), as illustrated in **Figure 9**. The band at 950–970 cm^{-1} was ascribed to the Q^2 units of Si–O–Si (Lodeiro et al., 2009). The vibration at about 1,160 cm^{-1} derived from quartz and mullite disappeared at 3 and 28 days, indicating the consumption of raw materials by chemical activation. A weak band appeared at 1,374 cm^{-1} in the samples cured for 1 day, which was ascribed to Q^4 units of Si–O–Si derived from FA. This band shifted to a lower wavenumber (1,340 cm^{-1}) when the samples were cured for 28 days, implying a lower polymerization degree with curing age forward. This phenomenon became more visible as shown in **Figure 9B** as adding TS to the alkali-activated binder system, suggesting the alteration of the structure of reaction products. Q^2 units appeared at 977 cm^{-1} at 28 days of curing for the sample without TS, but it shifted to a higher wavenumber (994 cm^{-1}), indicating the higher degree of geopolymerization of the structure. From the aforementioned, it can be concluded that the substitution of TS to FA caused the promotion of the reaction of binder (Lee and van Deventer 2002).

3.3.3 SEM Morphology

Figure 10 exhibits the morphology of alkali-activated binder at 28 days of curing. For the reference sample without TS, the products with petal-like shape with the size of 2 μm were observed, and these particles were loosely packing (**Figure 10A**). When TS was added, plate-like structure was developed, and some unreacted fly ash particles were also observed (**Figure 10B**). It indicates that the consumption of TS particles was faster than that of FA particles as the binder was activated by alkali solution, providing more reaction products with a denser structure, therefore leading to a higher compressive strength of binder. However, several micro-cracks with approximately 2 μm in width were observed in the sample containing TS. This may be ascribed to the fact that the

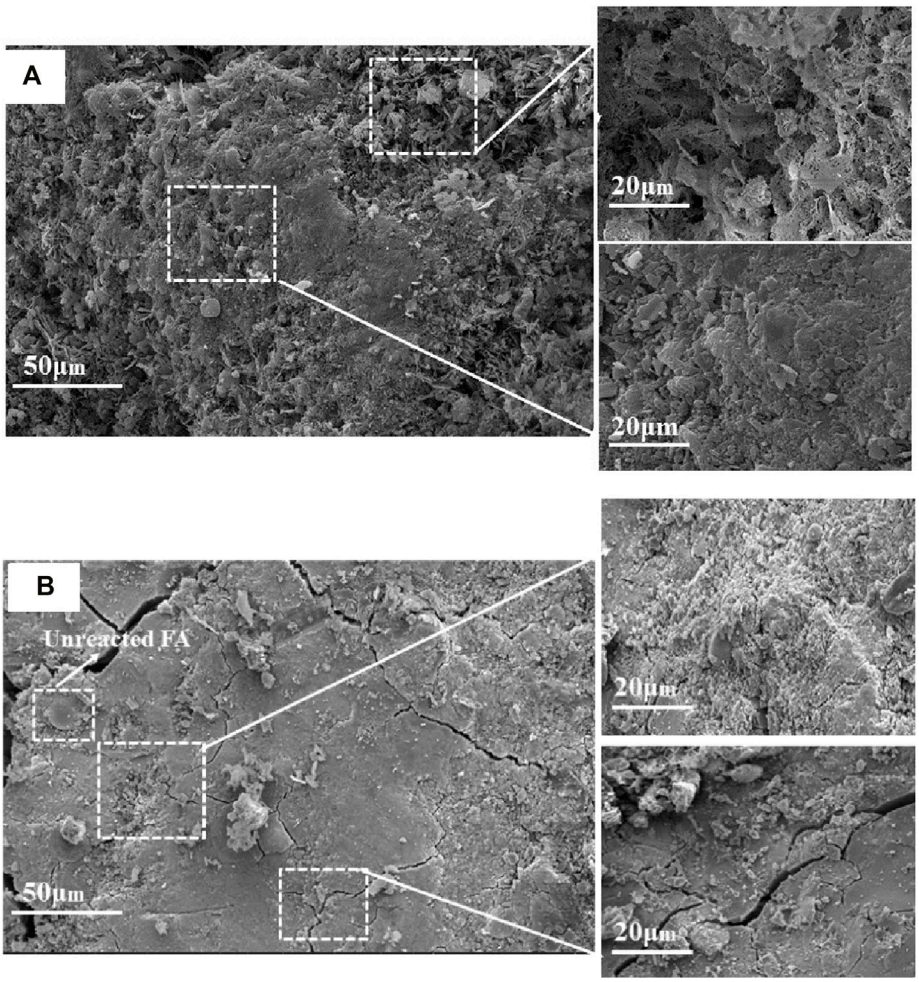

FIGURE 10 | SEM of alkali-activated binders with different compositions at different curing ages: **(A)** 70%FA:30%SG; **(B)** 30%FA:30%GGBS:40%TS.

addition of TS accelerated the reaction process of binder and promoted the formation of micro-cracks. Furthermore, the presence of TS produced a higher amount of C-(A)-S-H gel, which contained more adsorbed water molecules to maintain its shape. The drying shrinkage of the binder occurred after the removal of water molecules during the drying process, and it caused the formation of micro-cracks.

4 CONCLUSION

In this study, the reactivity of the extracted titanium tailings slag was improved by mechanical grinding, and the influence of the ground extracted titanium tailings slag on the setting and hardening properties of the alkali-activated FA-GGBS was investigated. The conclusions can be drawn as follows.

The particle size distribution of extracted titanium tailings slag (TS) can be optimized via mechanical grinding; as a result, the specific surface area and reactivity index were improved. The highest 28-day reactivity index was achieved at 15 min of grinding, and the value was 81.18%. Its average grain diameter of D_{50} and D_{90} were 48.31 and 82.89 μm, respectively.

No notable reduction in the fluidity of the alkali activated binder appeared as the replacement ratio of TS to FA increased to 40%, but it decreased dramatically at a higher replacement ratio.

The setting time of alkali-activated FA-GGBS was greatly reduced by the addition of TS due to the increased calcium content in the ternary binder, while the compressive strength of alkali-activated cementitious materials was increased first and then decreased with the increase of TS content. When the TS content was 40%, the early strength of the binder developed rapidly to 18.8 MPa, increased by 80.77% compared with the binder without TS, and the compressive strength at 28 days increased by 21.18% to 49.3 MPa.

The replacement of FA by TS could accelerate the reaction process and the main reaction products were C-(A)-S-H and gismondine. Adding TS in the binder increased the amount of C-(A)-S-H and improved the polymerization degree of hydration products. Meanwhile, the structure became more compacted, and thus the compressive strength of the binder was improved.

DATA AVAILABILITY STATEMENT

The original contributions presented in the study are included in the article/Supplementary Material; further inquiries can be directed to the corresponding author.

AUTHOR CONTRIBUTIONS

SW: conceptualization, methodology, writing—original draft. JL: validation, data curation. XY: methodology, validation. YZ: preparation of raw materials. XL: writing—original draft. ZZ: methodology, supervision, writing—review and editing.

FUNDING

This study was supported by the Natural Science Foundation Project of Chongqing (cstc2020jcyj-msxmX0954, cstc2020jcyj-msxmX0901), 111 Project of China (B18062), the National Natural Science Foundation of China (52078083), and the Fundamental Research Funds for the Central Universities (2020CDJ-LHZZ-088, 2021CDJQY-008).

ACKNOWLEDGMENTS

The authors gratefully appreciate the support from the Electron Microscope Center of Chongqing University (202103150147) and the project of Leading Talent of Science and Technology Innovation in Chongqing.

REFERENCES

Ameri, F., Shoaei, P., Zareei, S. A., and Behforouz, B. (2019). Geopolymers vs. Alkali-Activated Materials (AAMs): A Comparative Study on Durability, Microstructure, and Resistance to Elevated Temperatures of Lightweight Mortars. *Construction Building Mater.* 222, 49–63. doi:10.1016/j.conbuildmat.2019.06.079

Beltrame, N. A. M., Angulski da Luz, C., Perardt, M., and Hooton, R. D. (2020). Alkali Activated Cement Made from Blast Furnace Slag Generated by Charcoal: Resistance to Attack by Sodium and Magnesium Sulfates. *Construction Building Mater.* 238, 117710. doi:10.1016/j.conbuildmat.2019.117710

Biricik, H., Kırgız, M. S., Galdino, A. G. d. S., Kenai, S., Mirza, J., Kinuthia, J., et al. (2021). Activation of Slag through a Combination of NaOH/NaS Alkali for Transforming it into Geopolymer Slag Binder Mortar - Assessment the Effects of Two Different Blaine Fines and Three Different Curing Conditions. *J. Mater. Res. Tech.* 14, 1569–1584. doi:10.1016/j.jmrt.2021.07.014

Bumanis, G., Vitola, L., Bajare, D., Dembovska, L., and Pundiene, I. (2017). Impact of Reactive SiO 2/Al 2 O 3 Ratio in Precursor on Durability of Porous Alkali Activated Materials. *Ceramics Int.* 43, 5471–5477. doi:10.1016/j.ceramint.2017.01.060

Chindaprasirt, P., Chareerat, T., Hatanaka, S., and Cao, T. (2011). High-Strength Geopolymer Using Fine High-Calcium Fly Ash. *J. Mater. Civ. Eng.* 23, 264–270. doi:10.1061/(ASCE)MT.1943-5533.0000161

Chindaprasirt, P., De Silva, P., Sagoe-Crentsil, K., and Hanjitsuwan, S. (2012). Effect of SiO2 and Al2O3 on the Setting and Hardening of High Calcium Fly Ash-Based Geopolymer Systems. *J. Mater. Sci.* 47, 4876–4883. doi:10.1007/s10853-012-6353-y

Cui, C., Peng, H., Liu, Y., Zhang, J., Cai, C., and Peng, A. (2017). Influence of GGBFS Content and Activator Modulus on Curing of Metakaolin Based Geopolymer at Ambient Temperature. *J. Build Mater.* 20, 535–542. doi:10.3969/j.issn.1007-9629.2017.04.008

García Lodeiro, I., Macphee, D. E., Palomo, A., and Fernández-Jiménez, A. (2009). Effect of Alkalis on Fresh C-S-H Gels. FTIR Analysis. *Cement Concrete Res.* 39, 147–153. doi:10.1016/j.cemconres.2009.01.003

GB/T 1346 (2011). *Technical Specification for Test Methods for Water Requirement of normal Consistency, Setting Time and Soundness of the Portland Cement*. Beijing: China standard press.

GB/T 1596 (2017). *Technical Specification for Fly Ash Used for Cement and concrete*. Beijing: China standard press.

GB/T 17671 (1999). *Technical Specification for Method of Testing Cements-Determination of Strength*. Beijing: China standard press.

GB/T 8074 (2008). *Technical Specification for Testing Method for Specific Surface of Cement-Blaine Method*. Beijing: China standard press.

GB/T 8077 (2000). *Technical Specification for Methods for Testing Uniformity of concrete Admixture*. Beijing: China standard press.

Hong, Y. (2014). *Preparation and Properties of Alum Inoferrite Cement Clinker Based on the Slag of Ti-Si-V-Fe alloy-making from Titania-Rich BF Slag*. Wuhan: Wuhan University of Science and Technology. doi:10.7666/d.Y2657482

John, S. K., Nadir, Y., and Girija, K. (2021). Effect of Source Materials, Additives on the Mechanical Properties and Durability of Fly Ash and Fly Ash-Slag Geopolymer Mortar: A Review. *Construction Building Mater.* 280, 122443. doi:10.1016/j.conbuildmat.2021.122443

Kumar, S., Mucsi, G., Kristály, F., and Pekker, P. (2017). Mechanical Activation of Fly Ash and its Influence on Micro and Nano-Structural Behaviour of Resulting Geopolymers. *Adv. Powder Tech.* 28, 805–813. doi:10.1016/j.apt.2016.11.027

Kuri, J. C., Khan, M. N. N., and Sarker, P. K. (2021). Fresh and Hardened Properties of Geopolymer Binder Using Ground High Magnesium Ferronickel Slag with Fly Ash. *Construction Building Mater.* 272, 121877. doi:10.1016/j.conbuildmat.2020.121877

Lee, W. K. W., and van Deventer, J. S. J. (2002). The Effects of Inorganic Salt Contamination on the Strength and Durability of Geopolymers. *Colloids Surf. A: Physicochemical Eng. Aspects* 211, 115–126. doi:10.1016/S0927-7757(02)00239-X

Li, S., Li, Y., Xing, L., Ke, C., and Li, N. (2010). Porous Ceramics of Calcium Hexaluminate-Magnesia Alumina Spinel Prepared by Titanium Recovering Slag. *Refractories* 44, 100–103. doi:10.3969/j.issn.1001-1935.2010.02.006

Liu, W., Lin, L., Wang, S., Peng, X., Wu, B., Sun, K., et al. (2020). Setting and Hardening Behaviour of Alkali-Activated Landfilled Fly Ash-Slag Binder at Room Temperature. *Materials* 13, 3130. doi:10.3390/ma13143130

Liu, Y., Zhu, W., and Yang, E.-H. (2016). Alkali-activated Ground Granulated Blast-Furnace Slag Incorporating Incinerator Fly Ash as a Potential Binder. *Construction Building Mater.* 112, 1005–1012. doi:10.1016/j.conbuildmat.2016.02.153

Moghadam, M. J., Ajalloeian, R., and Hajiannia, A. (2019). Preparation and Application of Alkali-Activated Materials Based on Waste Glass and Coal Gangue: A Review. *Construction Building Mater.* 221, 84–98. doi:10.1016/j.conbuildmat.2019.06.071

Mucsi, G., Kumar, S., Csőke, B., Kumar, R., Molnár, Z., Rácz, Á., et al. (2015). Control of Geopolymer Properties by Grinding of Land Filled Fly Ash. *Int. J. Mineral Process.* 143, 50–58. doi:10.1016/j.minpro.2015.08.010

Nath, P., and Sarker, P. K. (2014). Effect of GGBFS on Setting, Workability and Early Strength Properties of Fly Ash Geopolymer concrete Cured in Ambient Condition. *Construction Building Mater.* 66, 163–171. doi:10.1016/j.conbuildmat.2014.05.080

Nath, P., Sarker, P. K., and Rangan, V. B. (2015). Early Age Properties of Low-Calcium Fly Ash Geopolymer Concrete Suitable for Ambient Curing. *Proced. Eng.* 125, 601–607. doi:10.1016/j.proeng.2015.11.077

Nishanth, L., and Patil, D. N. N. (2021). Experimental Evaluation on Workability and Strength Characteristics of Self-Consolidating Geopolymer concrete Based on GGBFS, Flyash and Alccofine. *Mater. Today Proc.* doi:10.1016/j.matpr.2021.10.200

Pavithra, P., Srinivasula Reddy, M., Dinakar, P., Hanumantha Rao, B., Satpathy, B. K., and Mohanty, A. N. (2016). A Mix Design Procedure for Geopolymer concrete with Fly Ash. *J. Clean. Prod.* 133, 117–125. doi:10.1016/j.jclepro.2016.05.041

Rakngan, W., Williamson, T., Ferron, R. D., Sant, G., Juenger, M. C. G., and Juenger, G. (2018). Controlling Workability in Alkali-Activated Class C Fly Ash. *Construction Building Mater.* 183, 226–233. doi:10.1016/j.conbuildmat.2018.06.174

Song, W., Zhu, Z., Peng, Y., Wan, Y., Xu, X., Pu, S., et al. (2019). Effect of Steel Slag on Fresh, Hardened and Microstructural Properties of High-Calcium Fly Ash Based Geopolymers at Standard Curing Condition. *Construction Building Mater.* 229, 116933. doi:10.1016/j.conbuildmat.2019.116933

Soutsos, M., Boyle, A. P., Vinai, R., Hadjierakleous, A., and Barnett, S. J. (2016). Factors Influencing the Compressive Strength of Fly Ash Based Geopolymers. *Construction Building Mater.* 110, 355–368. doi:10.1016/j.conbuildmat.2015.11.045

Sun, K. K., Xuan, D. X., Li, J. J., Ji, G. X., Poon, C. S., Wang, S. P., et al. (2022). Effect of the Ti-extracted Residue on Compressive Strength and Microstructural Properties of Modified Cement Mortar. *Constr. Build Mater.* 320. doi:10.1016/j.conbuildmat.2021.126190

Temuujin, J., van Riessen, A., and MacKenzie, K. J. D. (2010). Preparation and Characterisation of Fly Ash Based Geopolymer Mortars. *Construction Building Mater.* 24, 1906–1910. doi:10.1016/j.conbuildmat.2010.04.012

Wang, P., Han, B., Han, Y., Ke, C., and Li, N. (2008). Research on Hydration Capability of Panzhihua Iron and Steel CO.BF Slag after Silicon-Titanium Alloy. *B Chin. Ceram. Soc.* 27, 1208–1211. doi:10.16552/j.cnki.issn1001-1625.2008.06.029

Xiang, J., Liu, L., Cui, X., He, Y., Zheng, G., and Shi, C. (2019). Effect of Fuller-fine Sand on Rheological, Drying Shrinkage, and Microstructural Properties of Metakaolin-Based Geopolymer Grouting Materials. *Cement and Concrete Composites* 104, 103381. doi:10.1016/j.cemconcomp.2019.103381

Yao, Y. (2019). *Study on Effect of Chloride Ion Curing in High Chlorine Extraction Titanium Tailings*. Anshan: University of Science and Technology Liaoning.

Yip, C. K., Lukey, G. C., and van Deventer, J. S. J. (2005). The Coexistence of Geopolymeric Gel and Calcium Silicate Hydrate at the Early Stage of Alkaline Activation. *Cement Concrete Res.* 35, 1688–1697. doi:10.1016/j.cemconres.2004.10.042

Zhang, J. (2018). *Investigation on Utilization of Ti-Extracted Residues and Red Gypsum for the Preparation of Construct Ion and Building Materials*. Mianyang: Southwest University of Science and Technology.

Zhang, J., Pan, G., and Yan, Y. (2021). Early Hydration, Mechanical Strength and Drying Shrinkage of Low-Carbon Alkali-Activated Ti-Extracted Residues-Fly Ash Cement and Mortars. *Construction Building Mater.* 293, 123517. doi:10.1016/j.conbuildmat.2021.123517

Zhu, H., Wang, P., Zhang, J., and Wang, B. W. (2011). Effects of Chlorination Titanium Blast Furnace Slag on Strength and Microstructure of Mortar. *J. Build Mater.* 14, 443–446. doi:10.3969/j.issn.1007-9629.2011.04.002

Zhu, H., Wang, P., Zhang, J., and Wang, B. W. (2010). Preparation of Bricks by Using Titanium-Extracted Pangang BF Waste Slag. *New Build Mater.* 37, 31–33. doi:10.3969/j.issn.1001-702X.2010.06.009

Conflict of Interest: YZ is employed by Pangang Group Engineering Technology Co., Ltd.

The remaining authors declare that the research was conducted in the absence of any commercial or financial relationships that could be construed as a potential conflict.

Publisher's Note: All claims expressed in this article are solely those of the authors and do not necessarily represent those of their affiliated organizations, or those of the publisher, the editors, and the reviewers. Any product that may be evaluated in this article, or claim that may be made by its manufacturer, is not guaranteed or endorsed by the publisher.